Mechanistic study of membrane disruption by antimicrobial methacrylate random copolymers by the single giant vesicle method

Manami Tsukamoto,^a Emanuele Zappala,^{b†} Gregory A. Caputo,^c Jun-ichi Kikuchi,^a

Kayvan Najarian,^b Kenichi Kuroda*,^c Kazuma Yasuhara*,^{a, e}

- a) Division of Materials Science, Graduate School of Science and Technology, Nara
 Institute of Science and Technology, 8916-5 Takayama, Ikoma, Nara 6300192,

 Japan. E-mail: yasuhara@ms.naist.jp; Fax: +81-743-72-6099; Tel: +81-743-72-6091
- b) Department of Computational Medicine and Bioinformatics, University of Michigan,
 Ann Arbor, MI 48109-2800, U.S.A.
 - c) Department of Chemistry and Biochemistry, Rowan University, Glassboro, NJ 08028, U.S.A.

- d) Department of Biologic and Materials Sciences, University of Michigan School of Dentistry, 1011 N. University Ave., Ann Arbor, MI 48109, USA. E-mail: kkuroda@umich.edu; Fax: +1-734-647-2110; Tel: +1-734-936-1440
- e) Center for Digital Green-innovation, Nara Institute of Science and Technology, 8916-5 Takayama, Ikoma, Nara 6300192, Japan.
- † Present address: Institute of Mathematics and Statistics, University of Tartu, Tartu, 51009, Estonia.

ABSTRACT

Cationic amphiphilic polymers have been a platform to create new antimicrobial materials which act by disrupting bacterial cell membranes. While activity characterization and chemical optimization have been done in numerous studies, there remains a gap in our knowledge on the antimicrobial mechanisms of the polymers, which is needed to connect their chemical structures and biological activities. To that end, we used a single giant unilamellar vesicle (GUV) method to identify the membrane-disrupting mechanism of methacrylate random copolymers. The copolymers consist of random sequences of aminoethyl methacrylate and methyl (MMA) or butyl (BMA) methacrylate, with low molecular weights of 1600 – 2100 g·mol⁻¹. GUVs consisting of 8:2 mixture of 1-palmitoyl-2-oleoyl-sn-glycero-3-phosphoethanolamine (POPE) and 1-palmitoyl-2-oleoyl-sn-glycero-3-phospho-(1'-rac-glycerol), sodium salt (POPG) and those with only 1-palmitoyl-2-oleoyl-sn-glycero-3-phosphocholine (POPC) were prepared to mimic the bacterial (*E. coli*) or mammalian membranes, respectively. The disruption of bacteria and mammalian

cell membrane-mimic lipid bilayers in GUVs reflected the antimicrobial and hemolytic activities of the copolymers, suggesting that the copolymers act by disrupting cell membranes. The copolymer with BMA formed pores in the lipid bilayer, while those with MMA caused GUVs to burst. Therefore, we propose that the mechanism is inherent to the chemical identity or properties of hydrophobic groups. The copolymer with MMA showed characteristic sigmoid curves of the time course of GUV burst. We propose a new kinetic model with a positive feedback loop in the insertion of the polymer chains in the lipid bilayer. The novel finding of alkyldependent membrane-disrupting mechanisms will provide a new insight into the role of hydrophobic groups in the optimization strategy for antimicrobial activity and selectivity.

1.INTRODUCTION

Membrane-active cationic amphiphilic polymers have been promising platforms to develop a new class of antimicrobials which are effective in treating antibioticresistant bacterial infections. The design of antimicrobial polymers has been based on mimicry of the chemical and biophysical traits of host-defense antimicrobial peptides (AMPs) which are a component of the innate immune system in the body. 1-⁵ AMPs are known to have cationic amphiphilic properties that act by disrupting bacterial cell membranes or target intracellular components. 6-9 Therefore, antimicrobial polymers are designed to have cationic and hydrophobic groups, providing a cationic amphiphilicity. The cationic groups of the polymers facilitate preferential binding to bacterial cell membranes which are highly negatively charged as compared to the mammalian cell membranes by electrostatic interactions. The hydrophobic groups are then inserted into the hydrophobic core of bacterial cell membranes, leading to membrane disruption and ultimately cell death. Therefore, the antimicrobial activity increases as the hydrophobicity of the polymers increases. However, high hydrophobicity of polymers also causes nonspecific binding to mammalian cell membranes, resulting in toxicity to human cells. Therefore, the basic principle of chemical optimization of antimicrobial copolymers is to find the right balance in monomer compositions between the cationic and hydrophobic groups of copolymers in order to maximize the antimicrobial activity and minimize the toxicity to human cells. Traditionally, random-sequenced liner copolymers were initially explored by employing a variety of molecular frameworks

including polymethacrylates¹⁰, polyacrylates,¹¹ polyacrylamides,¹² polyoxetanes,¹³ polyurethanes, 14 nylon-3 polymers, 15, 16 and polynorbornenes. 17 Recently, the polymer platforms have been extended to other polymer shapes/architectures and macromolecules by the virtue of polymer chemistry, which were aimed to mimic the amphiphilic patterns and structures of natural peptides and proteins as well as their functionalities. These approaches include sequence defined block copolymers, 18, 19 branched polymers,²⁰ polymer micelles, ²¹ single chain nanoparticles,²² and macroscopic gels. ²³⁻²⁵ Through the structural optimization of these synthetic polymers, several examples of non-toxic, potent antimicrobial polymers have been successfully developed. 12, 13, 15 Therefore, the design rule of the balance between cationic and hydrophobic groups has been further extended from the monomer compositions to structural patterns or three-dimensional conformations to achieve the desired biological activities. However, while these polymers showed promising antimicrobial activity and biocompatibility, the chemical optimization for potent activity is still based on trial-and-error, and it is difficult to predict their activities from the monomer composition and chemical structure of the polymers. In order to rationally design new antimicrobial polymers for targeted activities, we need to learn their molecular mechanism for a deeper understanding of the structureactivity relationship.

The studies on AMPs – a parent model of AMP-mimetic polymers, proposed several molecular mechanisms to describe their behavior to disrupt bacterial cell membranes. One mechanism is the pore-forming toroidal model in which AMPs

assembled to form membrane pores.^{7,26} Another mechanism is the carpet mechanism²⁷ in which AMPs accumulate on the cell membranes, causing membrane solubilization. These molecular mechanisms of AMPs have been realized by the single vesicle giant unilamellar vesicle (GUV) method. ²⁸ The size of GUVs ranges from a few to 50 µm, and thus, a single vesicle can be observed using optical microscopy, allowing in situ examination of spatial and time-dependent morphological changes of membranes. This contrasts with the conventional method using large unilamellar vesicle (LUVs) with 100-500 nm, which provides collective results because the solution containing a large number of LUVs is used for experiments. Taking the advantage of GUVs, the previous studies in literature identified the mechanisms of AMPs. For example, citropin²⁹, aurein²⁹ and gomesin³⁰ have been reported to act by the carpet mechanism. On the other hand, membrane lytic melittin³¹⁻³³ and some antimicrobial peptides including magainin-2³⁴⁻³⁷, LL-37³⁸ and maculatin²⁹ have been also reported to act by forming pores. Yamazaki and coworkers previously reported their pioneer work using the single GUV method to study the kinetic model of pore formation by magainin-2.34-37 They demonstrated that the pore formation of magainin-2 can be described by the two-stage transition model from the bound state to the pore-forming state,³⁶ and they also proposed the tension-induced mechanism for pore formation.³⁵ Huang and co-workers also studied the action of several membrane-active peptides including AMPs on GUVs. 32, ^{33, 38} They observed the morphological change of GUVs caused by AMPs in combination with a micropipette aspiration technique ^{32, 33}. This technique was able to quantify the expansion of membrane area as well as the volume change of the

GUVs due to the binding of melittin. GUVs have been used for several studies of synthetic amphiphilic polymers.³⁹ However, while the mechanistic studies are limited, studies by the single GUV method would provide new insight into the polymer's interactions with lipid bilayers.

The overarching goal of this study is to elucidate the membrane-disruption mechanism of antimicrobial polymers using the single GUV method. To that end, we selected methacrylate random linear copolymers with binary compositions of cationic and hydrophobic monomers, as their activities and optimization have been extensively studied, but the membrane-disrupting mechanism is not known. To the best of our knowledge, this is the first report on the mechanistic studies of antimicrobial polymers using GUVs. Therefore, the primary focus of the current report is to provide the biophysical basis of membrane-disruptive mechanisms, which can be used to guide the molecular design of antimicrobial polymers, rather than the biological or physiological relevance of the polymer's activities. Accordingly, we synthesized a set of random copolymers with different alkyl lengths (either methyl or butyl) in the side chains and varied composition of methyl side chains in order to investigate the relationship between the chemical structure, activity, and mechanism. Next, we determined the antimicrobial activity against Gram-negative *Escherichia coli* (*E. coli*) as a model bacterium and hemolytic toxicity against sheep erythrocytes. Using these results as a guide, we have investigated the lytic activity of these copolymers against GUVs composed of 8:2 mixture of 1palmitoyl-2-oleoyl-sn-glycero-3-phosphoethanolamine (POPE) and 1-palmitoyl-2oleoyl-*sn*-glycero-3-phospho-(1'-*rac*-glycerol), sodium salt (POPG) or those with 1-palmitoyl-2-oleoyl-*sn*-glycero-3-phosphocholine (POPC), which mimic the bacterial (*E. coli*) or mammalian cell membranes, respectively. Based on analysis of the reaction kinetics, we propose a new mechanistic model for GUV burst, which implements a positive feedback loop in the insertion of the copolymer chains in the lipid bilayer.

2. EXPERIMENTAL METHODS

- **2.1. Materials.** 1-palmitoyl-2-oleoyl-*sn*-glycero-3-phosphocholine (POPC), 1-palmitoyl-2-oleoyl-*sn*-glycero-3-phosphoethanolamine (POPE) and 1-palmitoyl-2-oleoyl-*sn*-glycero-3-phospho-(1'-*rac*-glycerol), sodium salt (POPG) were purchased from NOF Co. (Tokyo, Japan). Melittin from honey bee venom and Rhodamine B isothiocyanate-dextran (RITC-dextran, average MW: 70 kDa) were purchased from Sigma-Aldrich Co. (MO, USA). Magainin 2 was purchased from AnaSpec (San Jose, CA, USA). Sheep whole blood was obtained from Japan Lamb, Ltd. (Hiroshima, Japan). All other chemicals were obtained from Wako Pure Chemical Industries, Ltd. (Osaka, Japan) and used without further purification.
- **2.2. Polymer synthesis and characterization.** The copolymers were synthesized and characterized according to our previous reports. ¹⁰ The molecular weight or the degree of polymerization of the polymers have been controlled by the addition of the chain transfer agent, methyl 3-mercaptopropionate (MMP). The degree of polymerization (DP) and the mole fraction of monomers of the copolymers were

calculated from the integrated areas in the NMR spectra. The number average molecular weights of the copolymers were calculated using DP, mole fraction of monomers, and the molecular weights of monomers and chain transfer agent. The experimental details for the polymer synthesis and characterization are provided in Supporting Information.

2.3. Antimicrobial assay. The antimicrobial activity of the copolymers was evaluated by the minimum inhibitory concentration (MIC) in which the polymers inhibit the bacterial growth completely. The MIC values of polymers were determined by a turbidity-based microdilution assay. 40 The overnight culture of *E.* coli ATCC 25922 in Muller-Hinton (MH) broth at pH 7.4 was diluted to OD of 0.1 and grown again to the mid-logarithmic phase ($OD_{600} = 0.5-0.6$). The bacterial culture was then diluted to give a stock suspension of $OD_{600} = 0.001$, which corresponds to $\sim 2 \times 10^5$ cfu/mL. This bacterial stock suspension (90 µL) was then mixed with a polymer solution (10 µL) containing polymer in two-fold serial dilutions in a sterile polypropylene 96-well plate (Corning #3359), which is not treated for tissue culture. The highest polymer concentration tested was 1,000 µg/mL. The plates were incubated at 37 °C for 18 hours without shaking. The OD₆₀₀ of each well was then read by a microplate reader, and an increase in turbidity from the MH broth control was considered as E. coli growth. The MIC values were determined below the solubility limits of polymers at which the polymers precipitate in MH broth. The MIC values of lytic peptide melittin and naturally occurring AMP magainin-2 were

also measured for comparison. The experiments were repeated in three times from bacterial growth.

2.4. Hemolysis assay. Hemolytic activity of the polymers was evaluated as the polymer concentration that induce the leakage of 50% hemoglobin from red blood cells (RBCs) (HC₅₀). Sheep whole blood (1 mL) were dispersed into phosphate buffered saline (9 mL) (PBS, 10 mM phosphate, 150 mM NaCl, pH=7.4) and then centrifuged at 1000 rpm for 5 min. The supernatant was removed using a pipette. The RBCs were then washed with PBS by repeating the same procedure two additional times. The obtained RBC stock suspension (10% v/v RBC) was diluted three-fold in PBS to give the assay stock. The assay stock (90 µL) was then mixed with the polymer solutions (10 μ L) prepared in the antimicrobial assay. The final concentration of RBCs on a 96-well microplate is 3% v/v. PBS solution (10 μL) or 1% v/v Triton X-100 (10 μL) was added instead of polymer solutions as negative and positive hemolysis controls, respectively. The plate was placed in an orbital shaker at 37 °C and 250 rpm for 60 min. The plate was then centrifuged at 1,000 rpm for 10 min. The supernatant (10 μL) was diluted into PBS (90 μL) and the absorbance at 405 nm was measured using a microplate reader. The fraction of hemolysis was calculated as the absorbance reading divided by the average of readings from the positive control wells. Hemolysis was plotted as a function of polymer concentration, and the experimental data was fitted to a function of the form H = $1/\{1+(HC_{50}/[P])^n\}$, where H is the fraction of hemolysis measured and [P] is the total concentration of polymer. The fitting parameters, n and HC_{50} are the Hill coefficient and the polymer concentration causing 50% of hemolysis, respectively.

These parameters of melittin and magainin-2 were also estimated for comparison.

The experiments were repeated for three times.

2.5. GUV preparation and microscopic observation. GUVs were prepared by the gentle hydration method.⁴¹ For the preparation of GUVs, POPE / POPG mixture (8:2) or POPC lipids were used to mimic a *E. coli* and mammalian membranes, respectively. Chloroform solutions of lipids were placed in a round-bottom test tube, and the solvent was evaporated *in vacuo* for 3 hours to form a thin lipid film. The obtained lipid film was gently hydrated with sucrose solution (200 mM) at room temperature for overnight. The resulting vesicular dispersion (6 µL) was added to glucose solution (200 mM, 143 µL) to give a contrast in between inner and outer phases of the GUV. Osmolarities of the sucrose and glucose solutions were adjusted to the same value to eliminate osmotic pressure imbalance in between outside and inside the vesicles. A series of microscopic images was acquired using an Olympus IX71 inverted optical microscope (Tokyo, Japan) equipped with x100 objective lens using a phase contrast and epifluorescence modes. Microscopic images were recorded using a Hamamatsu ORCA-Flash 2.8 CMOS camera (Hamamatsu, Japan). For the microscopic observation, we have used a hand-made chamber with dimension of 18 mm x 5 mm x 120 µm (Fig. S1 in Supporting Information). To the 15 μL of the GUVs suspension in a glucose solution placed in the camber, 1 μL of the polymer stock was injected using a Narishige IM-9B micropipette (Tokyo, Japan). The injection of the polymer stock was completed within 1 second. The pressure of

the injection was not controlled precisely as the micropipette was manually operated. The injection pipette was placed approximately 100 µm away from the target vesicle to minimize the time needed for the polymer to reach the GUV as well as the interference of the hydrodynamic disturbance due to the flow of solution. The time required for the injected solution to reach the GUV of interest that is estimated using fluorescent FITC-dextran (4kDa) is about 0.4 second (Fig. S2). Obtained images were analyzed using an Image | software. To quantify the release of the entrapped sucrose from GUVs, we have calculated the relative gray value as follows. The brightness of GUV inside and the outer aqueous phase in the phase contrast image were estimated by averaging the brightness of the circular regions of interest consisting of approximately 30,000 pixels each. Relative gray value was calculated by $(I_{out} - I_{in,t}) / (I_{out} - I_{in,0})$ where I_{out} , $I_{in,0}$, and $I_{in,t}$ are the values of brightness corresponding to outside of the GUV, the inside of the GUV before the addition of polymer, and time t after the addition of polymers, respectively. To obtain a calibration curve, a series of GUV samples containing different fractions of sucrose diluted with glucose solution were prepared, and the relative gray values were measured under a microscope as described above. The calibration curve indicated that the relative gray values is proportional to the sucrose fraction in the GUVs (Fig. S3)

3. RESULTS

3.1. Design and synthesis of cationic amphiphilic methacrylate copolymers.

Using previously published methods, we synthesized a set of methacrylate

copolymers containing primary ammonium groups and hydrophobic groups in the side chains. These copolymers have either methyl (PM₃₄ and PM₅₇) or butyl (PB₃₆) as hydrophobic side chains (Fig. 1) 10, and two different compositions (34 and 57) mol.%) of methyl side chains (methyl methacrylate). Compositional variation was designed to investigate the effect of the hydrophobic monomer composition and the side chain hydrophobicity on the antimicrobial activity and selectivity as well as the membrane-disruption mechanism of the copolymers. The copolymers were synthesized in the presence of chain transfer agent methyl 3-mercaptopropionate (MMP) to give relatively low molecular weights of 1,500 – 2,100 g·mol⁻¹, which are similar to those of AMPs. In general, the thiol group of MMP terminates the propagation of radial polymerization, but the chain termination generates a new thiyl radical, which initiate new polymerization.⁴² Therefore, the molecular wight of polymers depends on the mole ratio of the monomer to MMP. This chain transfer process is repeated until all the monomers are consumed, resulting in high yield of polymers with target molecular weights. The degree of polymerization (DP) in Table 1 represents the average number of monomer units in a polymer chain, and these polymers have DP of 12-15. It should be noted that our polymers are supposed to be called oligomers because of small molecular size in the polymer science field. However, peptide assemblies with defined structures are generally called as 'oligomers' in the field of peptide science. While our study mimic peptides, our polymers do not have any defined sequence nor structures. Thus, in this study, we denote our materials as 'polymers' to avoid confusion.

Figure 1. Synthesis of cationic amphiphilic methacrylate random copolymers

Table 1. Characterization of methacrylate copolymers, and antimicrobial and hemolytic activities.

Polyme r	DP ^a	$R^{ m b}$	$f_{ m HB}^{ m c}$	$N_{ m HB}^{ m d}$	Net charge	M_n (NMR) e (g·mol $^{-1}$)		Hemolysis at MIC (%)	HC ₅₀ (μg·mL ⁻¹)
P ₀	12	-	0	0	+12	1700 (3000)	>1000	-	>1000 (16 ±2.2 %) ^f
PM ₃₄	12	Methyl	0.34	4.1	+7.9	1600 (2500)	250	6.7 ± 2.2	>1000 (24±1.6 %) ^f
PM ₅₇	15	Methyl	0.57	8.6	+6.4	1800 (2500)	3.9	4.8±0.3	>1000 (48%±16 %) ^f
PB ₃₆	15	Butyl	0.36	5.4	+9.6	2100 (3200)	7.8	106±0.1	1.0

- a) Degree of polymerization, determined by ¹H NMR analysis.
- b) The hydrophobic side chain of polymers
- c) The mole fraction of hydrophobic side chains
- d) The average fraction of monomer units with hydrophobic side chains (methyl methacrylate or butyl methacrylate) in a polymer chain relative to the total number of monomers in a polymer chain.
- e) M_n was calculated using the molecular weights of monomers, MMP, and DP. The M_n value is based on the chemical structure without TFA. The M_n of polymers with TFA were given in the parenthesis.
- f) When the HC_{50} value was greater than 1000 μ g·mL⁻¹, the hemolysis % at 1000 μ g·mL⁻¹ is given in the parenthesis.

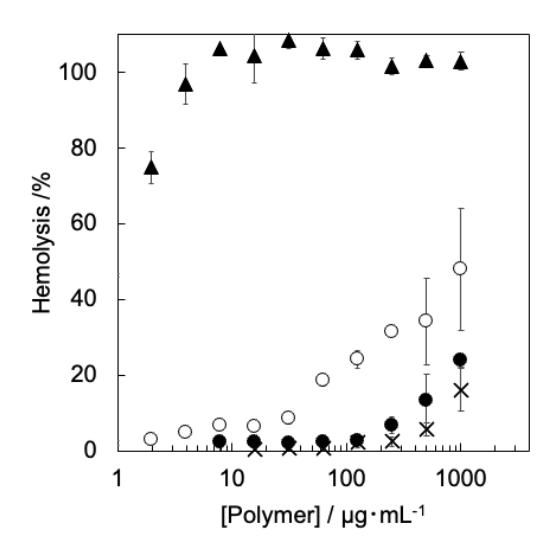


Figure 2. Concentration dependence of the hemolysis induced by P_0 (cross), PM_{34} (filled circle), PM_{57} (open circle), and PB_{36} (filled triangle). The data points and error bars represent the average and standard deviation of three experiments.

3.2. Antimicrobial and hemolytic activities. To assess the antimicrobial activity of the copolymers, the minimum inhibitory concentration (MIC) of the copolymers was measured against *E. coli*. The cationic homopolymer P_0 did not show any antimicrobial activity against *E. coli* (MIC >1000 $\mu g \cdot m L^{-1}$). The copolymers PM_{34} and PM_{57} showed antimicrobial activity with MIC values of 250 $\mu g \cdot m L^{-1}$ and 2.0 $\mu g \cdot m L^{-1}$, respectively. (Table 1) For comparison, naturally occurring AMP, Magainin 2 showed the MIC value of 125 $\mu g \cdot m L^{-1}$ under the same assay conditions. These results indicate that the antimicrobial activities of copolymers were increased as the fraction of methyl side chains in a polymer chain was increased, which is in good agreement with the previous report.⁴³ The copolymer PB_{36} showed higher activity

(MIC = $7.8 \, \mu g \cdot mL^{-1}$) than the counterpart polymer with methyl side chains PM₃₄ (MIC = $250 \, \mu g \cdot mL^{-1}$). This also supports the notion that the hydrophobicity of polymers drives the antimicrobial activity against *E. coli*.

On the other hand, the toxicity of copolymers to mammalian cells was evaluated as lytic (hemolytic) activity against sheep erythrocytes, which was evaluated by the amount of leaked hemoglobin (hemolysis %) relative to Triton X-100 as 100%. In general, the hemolysis % increased as the polymer concentration increased, and the hemolytic activity depends on the type of polymer. While the polymer concentration for 50% hemolysis (HC₅₀) has been used as a measure of hemolytic activity, P_0 and the copolymers with methyl side chains PM₃₄ and PM₅₇ showed < 50% hemolysis up to 1000 μg·mL⁻¹. However, at the polymer concentration of 1000 μg·mL⁻¹, P₀, PM₃₄ and PM₅₇ caused 16%, 24% and 48% of hemolysis, respectively (Table 1), indicating that the hemolytic activity was increased as the fraction of hydrophobic units in the copolymers was increased. Considering the use of the polymers as an antibiotic, it is important to know the safety of the polymers. PM₃₄ and PM₅₇ polymers induced very weak hemolysis at their MIC values (6.7 % and 4.8 % for PM₃₄ and PM₅₇, respectively). In contrast, PB₃₆ showed significant hemolytic activity, and the HC₅₀ was 1.0 μg·mL⁻¹, which is comparable to that of bee venom toxin melittin (MIC = 1.4 μg·mL⁻¹). Comparing the activities of PM₃₄ and PB₃₆, the increase in the alkyl length from methyl to butyl side chains significantly increased the antimicrobial and hemolytic activities of copolymers. These results are consistent with the previous finding that the hydrophobicity of copolymers increases both the antimicrobial and hemolytic activities.43

3.3. Disruption of bacterial membrane mimic-lipid bilayer. Here, we studied the lipid bilayer disruption mechanism of the copolymers using GUVs. In general, the E. coli cell membrane is rich in anionic phosphatidylglycerol (PG) and zwitterionic phosphatidylethanolamine (PE) lipids.⁴⁴ To mimic the lipid content and composition of *E. coli* cell membrane, GUVs were prepared using an 8:2 (molar ratio) mixture of POPE and POPG (Fig. 3). It should be noted that it would be ideal to use a physiologically relevant buffer and salt as well as ionic strength to investigate the biological relevance of the polymer mechanisms because these factors are likely to affect the polymers' action on the lipid bilayers. However, in general, GUVs were hardly produced with good reproducibility in ionic solutions due to the difficulty in the spontaneous hydration and detachment of the lipid film formed on the glass substrate, especially when zwitterionic POPC lipid is used.⁴⁵ POPC GUVs in ionic solutions including buffer have been prepared previously using polymer-assisted formation of GUVs⁴⁶ and the double emulsion method⁴⁷, which could be used for this study. However, these GUV samples would contain residual oil or polymers, and we were concerned that they may affect the polymer activities. In addition, the GUVs prepared in low salt concentrations cannot be diluted by a buffer solution such as PBS because the higher osmolarity of PBS would cause GUV breakage. To study the permeabilization of the lipid bilayer induced by the copolymers, membraneimpermeable sucrose was entrapped in the inside of GUVs as a leakage marker, while the outer buffer solution contains glucose.³⁰ Due to the difference in the refractive indexes between sucrose and glucose solutions, the inside of a vesicle

(sucrose) shows darker contrast than the outside (glucose) with a halo around the vesicle in a phase contrast image. Therefore, decreased darkness (gray value) inside the vesicle indicates the leakage of sucrose from the GUV ³⁶. Effectively, the more the "grayness" decreases in the vesicle, the more sucrose has leaked out. The fraction of sucrose in GUVs and the gray value relative to the outside showed a linear relationship (Fig. S3), suggesting that the relative gray value directly represents the concentration of sucrose remaining in the GUV, and the leakage curves by the polymers were not resulted from a non-linear relationship between the sucrose fraction and gray value. The osmolarities of glucose and sucrose solutions were measured and adjusted to be same (200 mOsm) in order to avoid the rupture of vesicles due to the imbalance of osmotic pressures across the lipid bilayer. The polymer solutions were added into the vicinity of a vesicle of interest using a micropipette so that the local concentration of polymers exposed to GUVs was expected to be close to that of the polymer stock solution.

Bacterial model

1-Palmitoyl-2-oleoyl-sn-glycero-3-phosphoethanolamine (POPE)

1-Palmitoyl-2-oleyl-sn-glycero-3-phospho-rac-(1-glycerol) Sodium Salt (POPG)

Mammalian model

1-Palmitoyl-2-oleoyl-sn-glycero-3-phosphocholine (POPC)

Figure 3. Chemical structures of phospholipids used in this study

As an initial attempt to probe into the polymers' behavior against GUVs, the fixed polymer concentration of $66.7~\mu g \cdot m L^{-1}$ was tested for all the polymers (Fig. 4). We have observed fluctuation in the relative gray value for P_0 and PM_{34} (Fig. 4A and B). The cause of fluctuation is not clear. While it cannot be ruled out, it is unlikely that the local change in the lipid bilayer by the polymers caused the fluctuation because the relative intensity was determined as the average values of the intensities from the whole region of the GUV inside. One possibility is that the fluctuation was caused by the movement of GUVs due to the convection currents of surrounding solutions, which might cause erratic intensities.

While the data points fluctuated, the cationic homopolymer P_0 did not cause any change in the morphology of bacterial model GUVs membrane, or release of entrapped sucrose over 16 minutes. On the other hand, PM_{34} -treated GUVs initially showed weak leakage of sucrose up to 10 % without any morphological changes, but they suddenly burst at the time of 12 minutes, and the entrapped sucrose was completely released into solution. To study the time-dependent dynamics of the membrane disruption caused by the polymers in detail, we have recorded the images of GUVs with fine-time resolution (Fig. S4) Spherical GUVs instantaneously disappeared within 0.2 second without showing any deformation of membrane such as the formation of wavy patterns, suggesting that the rapid burst of GUVs is the main mechanism of the membrane disruption for PM_{34} polymer. Since no aggregates or small vesicles were observed after the burst of vesicles, the polymer is likely to

disrupt membranes by forming small complexes with lipids that are not visible in the microscopy. A similar two-step action was also observed for PM₅₇ which showed sucrose leakage up to 10%, followed by the burst of GUV. There is no apparent difference in the GUV sizes or morphologies before the burst. These results suggest that PM₃₄ and PM₅₇ weakly permeabilized the lipid bilayer. While the mode of action is similar, these copolymers have distinctively different induction times to cause the burst of GUVs. The induction times were measured for approximately 50 GUVs, and the data showed a bell shape distribution with the maximum at the time of ~ 8 and \sim 3 minutes for PM₃₄ and PM₅₇, respectively (Fig. 5). It should be noted that the typical lifetime of the untreated GUVs was significantly longer (~hrs) than the time period (minutes) observed here. Therefore, the burst of GUVs can be attributed to the disruption of lipid bilayers by the polymers, but not to spontaneous rapture. The induction time results indicate that an increase in the mole fraction of methyl side chains increased the rate of the process of lipid bilayer rupture, but did not change the mechanism, i.e. burst of GUVs.

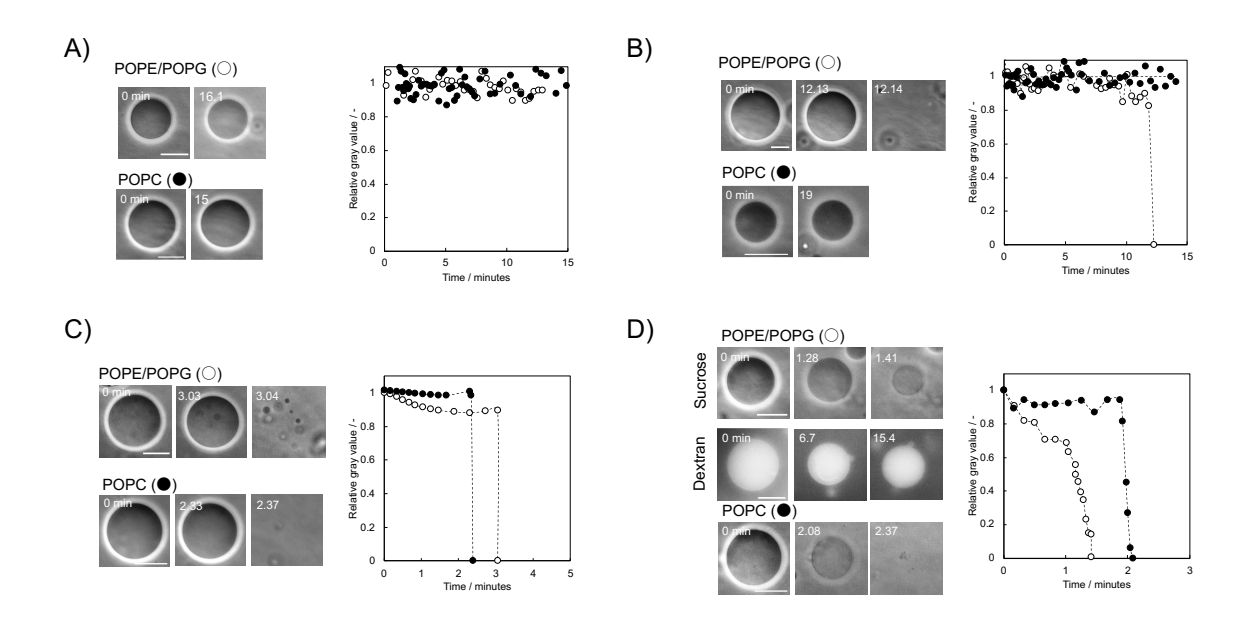


Figure 4. Disruption of GUV lipid bilayers by the methacrylate copolymers: A) P_0 , B) P_{34} , C) P_{57} , D) P_{36} . Representative data at 66.7 μ g·mL·1 were presented. POPE/POPG and POPC corresponds the lipid composition used for the preparation of bacterial (*E. coli*) and mammalian model GUVs, respectively. The images corresponding to the dextran leakage shown in the panel D were acquired by the florescence mode. The numbers in the top of each picture indicates the observation time of each GUV after the injection (in minutes). Bar = 10 μ m.

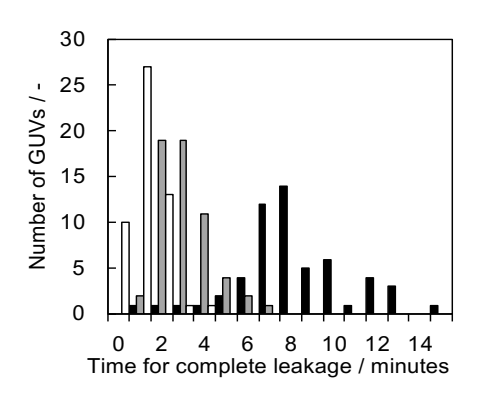


Figure 5. Induction time and accumulated fraction of burst or permeabilization of bacterial model GUVs. Distributions of induction time for GUV burst for PM_{34} and PM_{57} , and completion of sucrose leakage from GUVs for PB_{36} . (White: PB_{36} , Gray: PM_{57} , Black: PM_{34}) The induction time was measured for approximately 50 GUVs.

In order to determine if the lipid bilayer-disruption mechanism is dependent on the hydrophobic side chains, we also examined PB₃₆ for GUV lysis. Interestingly, GUVs started to release sucrose immediately after an addition of PB₃₆, which was concomitant with a shrinkage of the vesicle while its spherical shape maintained (Fig. 4D). The GUVs became completely empty within \sim 1.5 minutes (Fig. 4D). One possible explanation for the sucrose leakage is due to the transiently formed erratic defects in the lipid bilayers, which may cause permeation of relatively large molecules ^{48, 49}. Therefore, RITC-dextran (MW= 70 kDa, the hydrodynamic diameter of 12 nm, 10 μ M) and sucrose (MW = 342 g·mol⁻¹, the hydrodynamic diameter of 0.98 nm⁵⁰, 200 mM) were both entrapped in the same GUVs, which was treated by PB₃₆. The fluorescence intensity of RITC-dextran in the GUV remained constant after addition of PB₃₆ (Figs. 4D and S5), indicating no leakage of RITC-dextran, while sucrose leaked out. Interestingly, the PB₃₆ induced the budding of small vesicles from mother GUVs when RITC-dextran was entrapped with sucrose (Fig. 4D), but not when only sucrose was entrapped in GUVs. In some GUVs tested in the same experimental condition, we have observed that dextran was localized and retained in the mother vesicle after the formation of buds (Fig. S6). Although the detailed mechanism of the budding is the beyond the scope this paper, the PB₃₆ polymer is

likely to cause not only the disruption of membrane but macroscopic change of GUV shape.

The selective leakage of sucrose over dextran can be explained by the model that PB₃₆ formed size-limiting pores, which allow the passage of only small sucrose molecule (0.98 nm) through the lipid bilayer, but not large dextran polymer (12 nm). However, one may think that the dextran molecule could not diffuse out through the pores in the time frame (15.4 minutes) used in this study due to its high molecular weight (small diffusion coefficient) and low initial concentration, even though the pore diameter might be large enough, according to the Fick's law. Based on the Fick's law, the total area of the pore openings formed in the GUV membrane is 160 nm² for the sucrose leakage (Fig. 4D). (See Supporting Information for the calculation). Assuming that the dextran diffuses to the outside of GUVs through the same pores, 48% of the dextran should be released at the time of 15.4 minutes. However, we have not observed the decrease of fluorescence intensity inside the vesicle for 15.4 minutes after the addition of PB₃₆ (Fig. S5), indicating that no apparent leakage of dextran was not due to the slow diffusion. Taken together with the results of PM copolymers, the increase of alkyl length from methyl to butyl groups changed the lipid bilayer disruption mechanism of the copolymers from the rupture of lipid bilayer (a burst of GUVs) to the formation of size-limiting pores.

3.4. Concertation dependence of lipid bilayer disruption mechanisms. In order to determine if these observed bilayer disruption mechanisms are concentration-dependent, and thus these copolymers may possibly show both

mechanisms depending on their concentrations. To probe into this, the high polymer concentration (166.8 μg·mL⁻¹) was tested. All the polymers induced wavy patterns in the lipid bilayer in less than one minute after the addition of polymer solution (Fig. 6 and Fig. S7), and eventually the GUVs were completely disappeared. Sequential images with fine-time resolution showed that all the polymers disrupted GUVs in similar pathway regardless of the polymer structure starting with the formation of a wavy surface, followed by a partial dissolution, and finally complete disappearance of GUVs (Fig. S7). In addition, the formation of such wavy pattern was not observed at the polymer concentration of 66.7 μg·mL⁻¹ (Fig. S4). This may suggest that the GUV burst and pore formation at 66.7 μg·mL⁻¹ and the lysis at 166.8 µg⋅mL⁻¹ were driven by the different mechanisms. As the actin mode of GUV lysis was not dependent on the polymer structures, it is likely that the mode of action is non-specific. At the lower concentration of 6.67 μg·mL⁻¹, GUVs were intact without any sucrose leakage for PM₃₄ and PM₅₇ polymers. On the other hand, at 6.67 μg·mL⁻¹, PB₃₆ caused complete leakage of sucrose from GUVs, without any visible shrinkage of GUVs, suggesting pore formation. We have observed the same leakage behavior for three GUVs when treated with PB₃₆ at the same concentration whereas one GUV did not show the leakage at all. Based on these results, we found that the concentrations tested in this study is above the critical concentration of the polymer for the membrane permeation below that the polymer did not cause the leakage from any GUVs. These results suggest that GUV burst by the PM copolymers is likely to be the intrinsic mechanism of the PM copolymers. Similar to the PM copolymers, PB₃₆ also induced wavy patterns in the lipid bilayer at 166.8 μg·mL⁻¹, and formed

pores at 6.68 μ g·mL⁻¹. These results indicate that the pore formation is also inherent to PB₃₆.

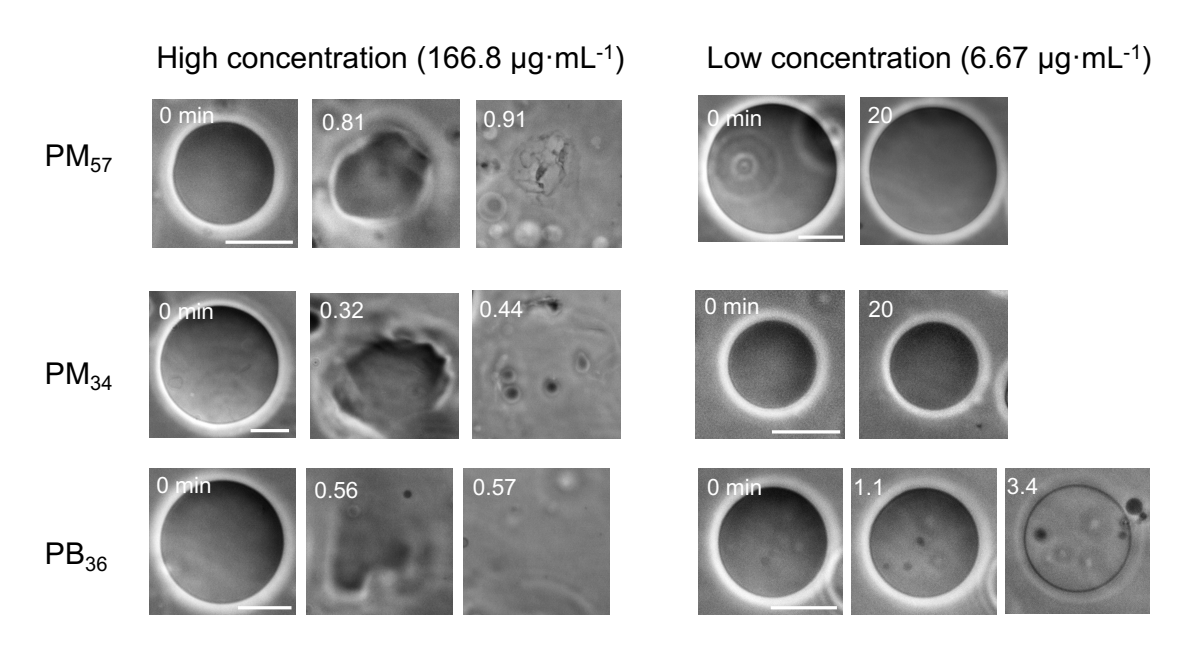


Figure 6. Disruption of POPE/POPG GUVs (bacterial membrane mimic) by the copolymers at high (166.8 μ g·mL⁻¹) and low (6.67 μ g·mL⁻¹) concentrations. The numbers in the top of each picture indicates the observation time of each GUV after the injection (in minutes). Bar = 10 μ m.

3.5. Disruption of mammalian cell membrane-mimic lipid bilayer in GUVs.

The toxicity of antimicrobial copolymers to human cells is a concern for their potential use as therapeutics. Here we investigated the effect of the copolymers on GUVs consisting of human cell membrane-mimic lipids. Because the major component of mammalian cell membrane is zwitterionic PC, we prepared GUVs consisting of 100% POPC (Fig. 3). The P_0 and PM_{34} , which show 16% and 24% hemolysis at 1,000 μ g·mL⁻¹ for P_0 and PM_{34} , respectively, did not cause sucrose

leakage from the human cell membrane-mimic POPC GUVs at 66.7 µg⋅mL-1 (Fig. 4A and B). These copolymers also did not cause any morphological change nor shrinkage of vesicles. One may think that the GUVs treated with PM₃₄ might be disrupted when incubated for a long time because PM₃₄ showed some hemolytic activity. However, the result for PM₃₄ was consistent when the experiments were repeated multiple times independently up to 60 minutes (Fig. S8). PM₅₇, which showed 48 % hemolysis at 1000 μg·mL⁻¹ higher than P₀ and PM₃₄, caused a slight leakage of sucrose up to 2 %, but the GUVs burst after certain induction time in similar to bacterial membrane mimic POPE/POPG GUVs (Fig. 4C). PM₅₇ did not change the size and morphology of the vesicles. On the other hand, highly hemolytic PB₃₆ (100 % hemolysis at 1000 μg·mL⁻¹) caused shrinkage of POPC GUVs concomitant with 10% leakage of sucrose for the first 2 minutes (Fig. 4D), and then sucrose was released with a high rate while the GUV shape was maintained. This result suggests that PB₃₆ also formed pores in POPC lipid bilayers. Taken together, the ability of the copolymers to disrupt or permeabilize the POPC lipid bilayer reflects the hemolytic activities of the copolymers. In addition, for PB₃₆ and PM₅₇ showed the same mode of mechanisms against both POPE/POPG and POPC lipid bilayers, indicating the mechanism is not dependent on the type of lipids.

3.6. Theoretical consideration for the GUV burst/permeation kinetics. We here attempt to construct a reaction model in order to shed light on the molecular mechanism of lipid bilayer disruption by the copolymers. We are particularly interested in PM_{34} and PM_{57} because of their characteristic induction times to cause

the bacteria-mimic GUVs to burst, which may provide an important clue to understand the underlying mechanism. For AMPs, several mechanistic models have been proposed to describe AMP-induced membrane disruption. The PM copolymers caused relatively low leakage of sucrose from GUVs initially and then a rupture of the lipid bilayer, resulting in a burst of the GUVs. We here propose the following mechanism to adopt AMP's "carpet model" in which accumulation of AMP chains causes rupture in a lipid bilayer, while other models assume pore formation in lipid bilayers (toroidal and stave-barrel models). Our previous molecular dynamic simulations suggested that the copolymer chains were attracted to the vicinity of surface of lipid bilayer through electrostatic interactions between the cationic side chains of the polymer and anionic lipid head groups of POPG.⁵¹ The polymer chains diffused through the vicinity of bilayer surface (P_{surf}), but they were not firmly bound to specific lipid heads which might be generally thought. In other words, the electrostatic interactions kept the polymer chains weakly associated with the surface of lipid bilayer. Then after certain period of time, the polymer chains in the surface vicinity were bound and inserted to the lipid bilayer through a hydrophobic pocket in the lipid bilayer, concomitant with the formation of amphiphilic conformations P_{ins} in which the cationic and hydrophobic side chains are segregated to the opposite sides of polymer chain backbone.⁵² This segregated amphiphilic conformation of P_{ins} is reminiscent of the cationic amphiphilic helices of AMPs which act by disrupting bacterial cell membranes. Therefore, presumably P_{ins} would be membrane-active, and thus permeate the lipid bilayer, which would be responsible for initial sucrose leakage in the GUV results. However, when the accumulation of

 P_{ins} reaches the threshold concentration, it would compromise the integrity of lipid bilayer structure, which cause rupture of lipid bilayer, followed by a burst of the GUV. Thus, the overall reaction scheme of the GUV - polymer interaction causing the burst of GUVs can be expressed as:

$$P_{surf} \xrightarrow{k_{ins}} P_{ins} \rightarrow \text{Membrane rupture, GUV burst - (1)}$$

We here consider that the burst of GUVs is the product of the whole reaction steps described in the model (Eq. 1). To obtain the reaction kinetic curve to analyze, we converted the number of GUVs with specific induction times (Fig. 5) to the accumulated fraction of GUVs that have burst, $F_{burst}(t) = N_{burst}(t) / N_0$, where N_{burst} (t) is the accumulated number of GUVs that have burst until the time of t, and N_0 is the total number of tested GUVs. Accordingly, in similar to chemical reaction kinetics, the time course of F_{burst} reflects the reaction kinetics for the formation of P_r (GUV burst) (Fig. 7). Interestingly, the time courses of F_{burst} (t) are sigmoidal in which the rate of increase in F_{burst} (the slope of curve) increases with time, but decreases as F_{burst} is close to the completion of reaction at long times. There have been several studies reporting sigmoidal curves for the concentration dependence of AMP activities. For example, maculatin and aurein peptides displayed sigmoidal concentration dependence on the dye leakage from vesicles mimicking mammalian and bacterial membranes.⁵³ The conformational change of alamethicin peptide upon the binding to membrane also showed sigmoidal concentration dependence.⁵⁴ The dose-response curve for the inhibition of bacterial growth by some cationic αhelical peptides consisting of leucine and lysine was also found to be sigmoidal. However, to best of our knowledge, there is no previous report of a sigmoid curve for vesicle rupture kinetics (time course) in previous AMP studies. In this study, we assume that the sigmoidal time dependence of GUV burst is stemmed from accumulation of the polymer chains with membrane-active conformations, with time. Therefore, the sigmoidal response found in this study may be inherent to the AMP-like activities. This non-linear kinetics prompted us to consider "an autocatalytic reaction" in the mechanism of polymer-induced lipid bilayer rapture. In general, autocatalytic reactions are those in which a product X catalyzes the formation of another product from a reactant X, as described in X + X - X. This reaction system with positive feedback typically gives sigmoid curves because the reaction starts from a small (seeding) amount of X.

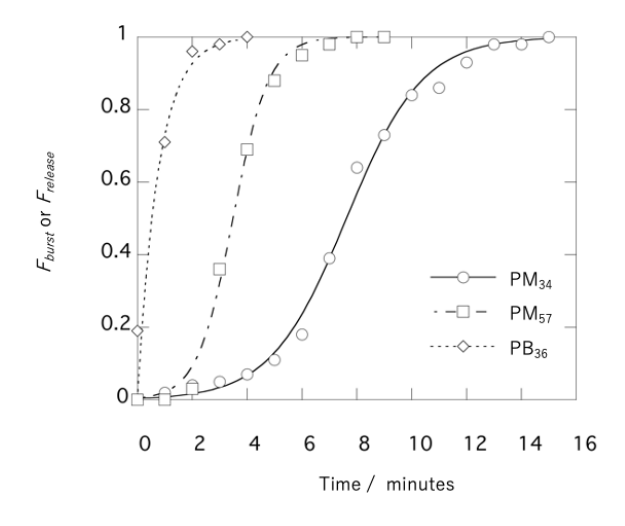


Figure 7. Time courses of the membrane disruption by the polymers. F_{burst} represents the accumulated number fraction of burst GUVs by PM₃₄ and PM₅₇ polymers. $F_{release}$ corresponds the accumulated number fraction of GUVs displaying the complete release of entrapped sucrose by PB₃₆ polymer.

Based on the mechanism model (Eq. 1), we further propose that the sigmoidal curves are a result of the positive feedback to the step of polymer chains P_{surf} in the vicinity of the bilayer surface to be inserted into the hydrophobic core of the lipid bilayer P_{ins} . We will discuss the molecular mechanism of auto-catalytic process in detail later. Accordingly, we hypothesize that the formation of P_{ins} is the rate determining step, and thus the accumulation (surface concentration) of P_{ins} on the lipid bilayer directly determine the time course of F_{burst} , or increase the probability of GUV burst as described as follows:

$$F_{burst} = b[P_{ins}] - (2)$$

where b is a scaling factor. The polymer aggregation with the positive feedback can be described by the following equation:

$$P_{surf} + P_{ins} \xrightarrow{k_{ins}} 2P_{ins} - (3)$$

where k_{ins} is the rate constant. The rate of the formation of P_{ins} can be written as follows;

$$\frac{d[P_{ins}]}{dt} = k_{ins} [P_{surf}] [P_{ins}] - (4)$$

[P_{ins}] is given by:

$$[P_{ins}] = \frac{[P_{surf}]_0 + [P_{ins}]_0}{1 + \frac{[P_{surf}]_0}{[P_{ins}]_0} e^{-(P_{surf}]_0 + [P_{ins}]_0)k_{ins}t}} = \frac{C}{1 + ae^{-Ck_{ins}t}} - (5)$$

where $[P_{surf}]_0$ and $[P_{ins}]_0$ are the initial concentrations of P_{surf} and P_{ins} , respectively, $C = [P_{surf}]_0 + [P_{ins}]_0$, and $a = [P_{surf}]_0 / [P_{ins}]_0$, and we have assumed $[P_{surf}]_0 + [P_{ins}]_0 = [P_{surf}]_0$ + $[P_{ins}]_0$, suggesting that the total polymer concentration on the bilayer does not change during the reaction. $[P_{ins}]_0$ represents the seeding quantity of membraneactive polymer chains P_{ins} , which initiate the catalytic insertion of the polymer chains on the lipid bilayer. Therefore, we expect $[P_{surf}]_0 >> [P_{ins}]_0$, or a >> 1 which will be confirmed later from the curve fitting results. It should be noted that, while it should take some time to reach the binding equilibrium of the polymers after polymer addition, we assume here that the time is significantly shorter than the induction times of GUV burst or negligible. Indeed, as the distance between the GUV and the micropipette was 100 µm, the time required for the polymer to reach the GUV was found to be less than one second (Fig. S2), while the GUV burst takes minutes (Fig. 5). Furthermore, previous studies reported that the time for the binding equilibrium of antimicrobial peptide magainin was estimated to be 2 seconds in similar GUV experiment, ³⁶ which also support our assumption.

From Equations (2) and (5), we obtain the following equation to describe F_{burst} :

$$F_{burst} = \frac{bC}{1 + ae^{-Ck_{ins}t}} - (6)$$

At infinite t, $F_{burst} \sim 1 = bC$. Therefore, b = 1/C. F_{burst} is finally given by the following simple form of equation:

$$F_{burst} = \frac{1}{1 + ae^{-kt}} - (7)$$

in which, $k = k_{ins}C$. This presents the specific case of a logistic function which has been used to characterize sigmoidal time dependence. ^{58,59} The equation (7) fits well to the F_{burst} data of PM₃₄ and PM₅₇, supporting our autocatalytic model. The values of a were 250 for PM₃₄ and 208 for PM₅₇, which are >> 1, indicating that only a small fraction of P_{surf} inserted into the lipid bilayer in the beginning of reaction. The k value of PM₅₇ (k = 1.53 min⁻¹) is larger than that of PM₃₄ (k = 0.72 min⁻¹).

On the other hand, the time course of $F_{release}$ for PB₃₆ steeply increased in the beginning of time and reached the completion within a few minutes, indicating that PB₃₆ forms pores in the lipid bilayer quickly without an induction period. The time course of PB₃₆ is similar to those of pore formation by natural AMP magainin 2.³⁶ Yamazaki and coworkers used the single GUV method to investigate the kinetics of pore formation by magainin 2 and demonstrated that the time course of the fraction of intact GUV ($F_{intact} = 1 - F_{burst}$) can be expressed by an exponential decay.³⁶ The

 $F_{release}$ data was also fit to an exponential function $(1 - \exp(-k_p t))$ (Fig. 7), where k_p is the rate constant. The value of k_p of PB₃₆ was 1.3 min⁻¹ at the polymer concertation of 21µM (66.7 µg·mL⁻¹), while the reported value for magainin 2 at 10 µM is 1.6 min⁻¹. It appears that the pore formation of magainin 2 and PB₃₆ are characterized by a similar order of time scale for activity (~minutes).

4. DISCUSSION

In this study, we determined the antimicrobial and hemolytic activities of methacrylate copolymers as well as the lytic activity against GUVs with lipid compositions which mimic the *E. coli* cell membrane (POPG/POPE) or mammalian cell membrane (POPC). A series of polymers examined in this study provide a range of antimicrobial and hemolytic activities (Table 1). In general, the copolymers that showed antimicrobial activity (PM₃₄, PM₅₇, and PB₃₆) against *E. coli* caused the permeabilization or rupture of *E. coli*-mimic lipid bilayer (POPG/POPE). On the other hand, the copolymers that showed hemolytic activity against sheep erythrocytes (PM 57 and PB36) also did the same action to the mammalian cell-mimic (POPC). While PM₅₇ and PB₃₆ showed relatively small MIC values against E. coli, they are very different in their hemolytic activities; PM₅₇ is antibacterial with a strong tendency to disrupt mammalian cells, which is selective to bacteria ($HC_{50} > MIC$), but PB₃₆ is much more a disruptor of mammalian cells than it is a selective antibacterial $(HC_{50} < MIC)$. These results suggest that the biomimetic lipid compositions of the GUVs reflect the biological activities of the copolymers against the target cell

membranes. Therefore, this supports our hypothesis that these copolymers act by disrupting cell membranes for their antimicrobial and hemolytic activities.

PM copolymers permeate the lipid bilayer and then caused GUV to burst after an induction time. To explain this, we proposed the AMP's carpet model-like mechanism in which the polymer chains are initially associated with the surface vicinity of lipid bilayer by electrostatic interactions (P_{surf}), and inserted into the hydrophobic core of the lipid bilayer to form the membrane-active amphiphilic conformation (P_{ins}). When the accumulation of inserted polymer chains reaches the threshold, the lipid bilayer would be ruptured. We also presumed that the inserted polymer chains permeabilize the lipid bilayer, causing leakage of sucrose before GUV burst. It has been previously demonstrated that AMPs form amphiphilic αhelices when they are bound to lipid bilayers. 60 The hydrophobic face is inserted into the outer leaflet of the lipid bilayer, which produces the asymmetry of the membrane tension between two leaflets, resulting in the disruption of membrane to translocate the peptide. 32, 61 Similar to AMPs, the binding of PM copolymers would also induce this imbalance between the outer and inner leaflet of lipid bilayer to permeabilize and disintegrate the lipid bilayer. In addition to AMPs, Riske and coworkers also reported that sodium dodecyl sulfate (SDS) adsorbed onto only outer leaflet of lipid bilayer, resulting in the burst of membrane with some induction time when the SDS concentration reached a critical value. 62 These previous studies support our proposed model for lipid bilayer permeation and rupture (GUV burst) by the copolymers. However, while our model assumes a simple mechanism, the

polymer insertion also involves complexation with lipid and other polymer chains. We will discuss the molecular roles of lipids and polymer chains in the membrane-disrupting mechanism later.

PB₃₆ caused a release of sucrose likely due to pore formation, but it was also concomitant with a shrinkage of the vesicle while any morphological changes including budding were not observed. In general, GUV shrinkage is induced by either hypertonic condition or a removal of lipids from the lipid bilayer or lipid solubilization. The former unlikely happened for our case because the GUV maintained the spherical shape, and the osmotic pressures inside and outside the vesicle were prepared to be the same. Here we hypothesize that the GUV shrinkage is due to the partial solubilization of the lipid bilayer by the PB₃₆ polymer chains, which reduces the total surface area of GUVs. Indeed, we have previously reported that the analogous methacrylate copolymers formed tens of nanometer-sized discoidal complexes (nanodiscs) with phospholipids. 63 These complexes are too small to observe under a microscope, and therefore, no visible particles or micelles could be found in the surround medium of polymer-treated GUVs. It has been reported that membrane lytic peptide, melittin similarly induces the release of entrapped sucrose with the shrinkage of GUVs.³¹ The solubilization of membranes by melittin results in the formation of small discoidal fragments of membrane that cannot be directly observed under a microscope.⁶⁴

At high polymer concertation of 168 µg·mL-¹, PM and PB copolymers induced transient wavy patterns in the lipid bilayer, followed by the disruption of GUVs. It has been reported that TX-100 also caused the transient formation of wavy patters in a lipid bilayer of GUVs. The formation of the wavy pattern was explained by the mechanism in which the insertion of the surfactant in the lipid bilayer expanded the surface area of lipid bilayer. Similarly, we speculate that the insertion of polymer chains would also increase the surface area of lipid bilayer, causing wavy patterns in the lipid bilayers. In addition, this action did not depend on the type of copolymers with different monomer compositions, which contrasts to the GUV response at lower polymer concentrations where the wavy pattern of the membrane was not produced. The high concentration of the polymers appears to offset the properties of the copolymers, and the surfactant-like mode of action may be dominant.

In this study, we used the same three polymer concentrations for our initial investigation of polymer-lipid bilayer interactions in the GUV experiments. We believe that the data from these three concentrations captured the framework of copolymers' behavior against the lipid bilayers as well as provide the biophysical basis for membrane-disrupting mechanisms. However, the selection of these polymer concentrations was rather arbitrary, and more systematic investigation would be needed to elucidate the concentration dependence of the polymer activities against GUVs and biological relevance of the mechanisms to the antimicrobial and hemolytic activities of copolymers. More specifically, the MIC and HC_{50} values depend on the monomer compositions of the copolymers; these values

decreased (the antimicrobial and hemolytic activities increased) as the hydrophobicity of the copolymers increased. The threshold concentrations of the copolymer to cause GUV burst or permeabilization are expected to reflect these values of polymers' biological activities. In addition, this study used a binary lipid mixture of POPE/POPG as well as POPC alone for GUVs as cell membrane mimics. The biological cell membranes contain many other components including lipids, proteins, and polysaccharides, different compositions, and cell wall or surface structures. Lipid composition in the membrane is known to affect the membrane disruption activity of AMPs. For example, cholesterol, which is abundant in mammalian cells, reduces the membrane activity of AMPs by rigidifying the membrane. 65 Cardiolipin found in *S. aureus* membrane also modulates the lytic activity of AMPs by increasing the lipid packing.⁶⁶ Further study using GUVs consisting of more complex lipid/protein compositions would be needed to link the polymer mechanism to their antimicrobial activity and toxicity to mammalian cells. It would be possible to use the GUVs formed by the lipids extracted from bacterial membrane⁶⁷ or erythrocyte ghost⁶⁸ as more relevant model membranes. Alternatively, GUVs directly produced from intact cells that consists of not only lipid but membrane proteins can be employed as a further realistic model membrane system.⁶⁹ Our previous study demonstrated that analogous methacrylate copolymers were also effective in killing other Gram-negative and Gram-positive bacteria.⁵² Because amphiphilic copolymers are designed to act by disrupting bacterial cell membranes, these polymers are expected to show a broad spectrum of activity. However, because the lipid compositions of bacterial membranes largely

varied for different bacteria, and the polymer's mode of action depends on the lipid compositions, we expect that the polymers would act differently against different bacterial membrane models. In addition, the observation time of GUVs in this study is up to 20 minutes, which is significantly shorter than the timeframe of antibacterial MIC assay (18 hours incubation). While we found a reasonable relationship between the GUV results and biological activities, the GUV experiments may not reflect the long-term effect of polymers on bacteria and mammalian cells. It will be needed to investigate more biologically relevant models and conditions as well as seek the biological relevance of the GUV data to the polymer activities to bacteria and mammalian cells in the future.

One of the key findings in this study is the dependence of the membrane-disrupting mechanism on the hydrophobic groups of the copolymers; PB₃₆ formed pores on the lipid bilayer of GUVs, and PM₃₄ and PM₅₇ caused GUVs to burst. These mechanisms are not dependent on the lipid types. These may suggest that the mechanism of the copolymers is inherent to the alkyl lengths of hydrophobic side chains. In the pore-forming model for AMPs, the hydrophobic domains of peptide helices are inserted into the lipid bilayer, and the cationic domains face the channel, which stabilize the pore structures. While the copolymers are not designed to form any secondary structures such as helices, the flexible polymer chains are likely able to adopt an amphiphilic conformation in which the alkyl chains are inserted into the lipid bilayer, and the cationic groups form a hydrophilic channel. If the pore structure with the polymer chains is stable, the morphology of GUVs would be

intact, but release the contents (sucrose) to the outer solution. Our previous study using sum frequency generation (SFG) spectroscopy on the analogous copolymers indicated that when inserted to the hydrophobic core of lipid bilayer, the butyl side chains were aligned with the lipid acyl chains, which indicate the butyl side chains can be inserted into the hydrophobic domain of lipid bilayer. To It has also been previously reported that acrylic acid copolymers with long alkyl side (C_8) chains form size-defined pores in a lipid bilayer, which is in good agreement with our finding here. On the other hand, while the PM polymers have different monomer fractions of methyl side chains, they both caused GUVs to burst. This may indicate that the lipid bilayer rupture is due to the property of methyl groups on the side chains, but not lack of sufficient overall hydrophobicity of the polymer chains. Based on the presented data, we hypothesize that the methyl side chains are too short to stabilize the pore structure, which requires further investigation to prove.

The sigmoidal time course of GUV burst also lends support our hypothesis on the weak hydrophobic interaction of methyl groups with the lipid bilayer. Based on the proposed model in Eq. 1, the polymer chains inserted into the lipid bilayer are membrane-active. The rate of the rupture kinetics is given by $k = k_{ins}([P_{surf}]_0 + [P_{ins}]_0)$, which reflect a combination of the rate of polymer insertion, k_{ins} and the initial concentration of inserted polymer chains $[P_{ins}]_0$ which act as a seed for the autocatalytic reaction. The k values of the PM copolymers are much smaller than that of PB₃₆. The weak hydrophobicity of methyl side chains may result in slower insertion to the hydrophobic domain of the lipid bilayer, resulting in small k_{ins} values

and thus small k values. On the other hand, the weak hydrophobicity of polymers may also result in the small amount of the inserted polymers $[P_{ins}]_0$ at the beginning, which was implicated by the large value of a (= $[P_{surf}]_0/[P_{ins}]_0$). Therefore, the weak hydrophobicity of polymers may result in either slow insertion or small amount of seed polymer chains, or both, leading to small k values. In contrast, while the GUV burst kinetics by PM polymers takes an order of minutes, PB₃₆ formed pores in the lipid bilayer immediately after addition to GUVs. This can be explained by the strong hydrophobicity of butyl side chains, allowing quick insertion into the hydrophobic domain of the lipid bilayer, resulting in the larger k value and lack of an induction period.

Why is the polymer insertion process autocatalytic? This might be explained by the polymer-induced formation of lipid clusters and hydrophobic defects at the boundaries. Epand and coworkers demonstrated that binding of cationic polymers induced lipid clusters or domains in bacterial membrane-mimics. Our previous study using computational simulations also showed that insertion of methacrylate copolymer chains induced clustering of POPG, and the polymer chains were bound to the boundary of the POPG cluster with POPE lipids, which provided hydrophobic defects due to the mismatch in bilayer thickness and intrinsic curvature between POPG and POPE domains. We speculate that the insertion of the PM copolymers into the GUV lipid bilayer also induced POPG clustering and created the hydrophobic pockets at the boundaries, which recruited another polymer chain into the bilayer, leading to the positive feedback loop in the polymer insertion. Therefore, POPG

lipids have dual roles in the polymer's membrane-disrupting mechanism: the anionic charge electrostatically attracts the cationic polymer chains to bring them to the vicinity of lipid bilayer surface, and the cluster of POPG generates hydrophobic pockets for the binding of the polymer chains at the boundary with POPE. In addition, the other lipid component POPE lipids have been indicated in previous studies to play key roles in the membrane-disruption mechanism of AMPs and antimicrobial polymers. The intrinsically negative curvature of PE lipids promotes the pore formation of AMPs and methacrylate copolymers in lipid bilayers. ⁷² The previous study using GUVs on Polybia-MP1 lytic peptide demonstrated that the membrane disruption by the peptide was enhanced when PE lipids were incorporated in the bilayer. ⁷³ PE lipid with small head group would modulate the topology of a binding site in the membrane in order to accommodate specific AMPs with a topologically matched amphiphilic structure. ⁷⁴ Our result may add another role of PE lipid as a "catalyst" in the membrane insertion of polymer chains in conjunction with PG lipids.

The results also provide a new insight into the basic design principles for antimicrobial copolymers. Our results indicate that the biological activities of the copolymers and their ability to disrupt lipid bilayers reflect the hydrophobicity of copolymers, which is in good agreement with previous studies.⁷⁵ The mainstream approach to structure optimization for antimicrobial copolymers with potent activity and selectivity is through testing a diverse range of different monomer compositions and hydrophobic groups in copolymers. However, our results suggest

that changing compositions of hydrophobic monomers (i.e. hydrophobic/cationic balance) and using different hydrophobic side chains are <u>not</u> equivalent in terms of the membrane-disruption activity. This may provide some explanation about why it is difficult to predict the antimicrobial activity and toxicity of copolymers from their chemical structures; we are likely to change the membrane-disrupting mechanism of copolymers when different hydrophobic side chains are used while we intend to tune the overall hydrophobicity of copolymers. This explanation has been speculated in the field, but not explicitly demonstrated in previous studies.

In this study, we examined only the effect of monomer compositions and hydrophilic groups on the polymer activities. However, the molecular weight of copolymers is also an important factor to control their antimicrobial and hemolytic activities. In general, the antimicrobial and hemolytic activities of methacrylate copolymers increased as the polymer molecular weight increased. However, the increase in the hemolytic activity is much more significant than antimicrobial activity, so that the high molecular weight polymers are highly toxic to mammalian cells and non-selective to bacteria. It would be of interest to use GUVs in order to investigate the membrane-disrupting mechanism of high molecular weight copolymers, which may provide some clues to understand why they are so highly toxic.

From the material-centric viewpoint, we can also interpret the results differently claiming that the membrane-disrupting mechanisms of synthetic copolymers can be readily switched by simple alternation of the alkyl length (methyl and butyl) of side chains. This contrasts with the relationship between AMP sequences and

mechanisms. Studies reported that some AMPs act by the pore-forming model, and others do by the carpet model.^{7, 27} However, there have been no specific amino acid sequences or motifs identified to predict or discriminate between these mechanisms. Interestingly, several studies also showed a parallel mechanism of AMP, and changing only 1-2 methylene groups changes its activity. ^{76,77,78} Therefore, it is not yet possible to predict the mechanism of AMPs from their sequences. However, our results indicate that we may be able to control the cell membrane permeation mechanism in polymers by design. The alkyl-dependent mechanism reported in this study may provide a new tool to study the relationship between the membrane-disrupting mechanism (pores or membrane rupture) of antimicrobial copolymers and bacterial response (antimicrobial activity). In addition, one may wonder how the finding of this study can contribute to maximize the antimicrobial activity of polymers while minimizing their hemolytic/cytotoxic activity. One possible outcome is, for example, although we used only methyl and butyl groups, we may be able to tune the chemical structure and composition of the hydrophobic side chains as to enhance the hydrophobic insertion of polymer chains into the bacterial membrane for the quick and effective formation of membraneactive P_{ins} , which would lead to potent antimicrobial activity. If the polymer insertion to the hydrophobic core of the membranes is selective to the bacterial lipids such as PE and PG lipids, the selective activity to bacteria over human cells would be further improved.

5. CONCLUSION

In summary, we used the single GUV method to study the membrane-disrupting mechanism of methacrylate random copolymers. The disruption of bacteria and mammalian cell membrane-mimic lipid bilayer in GUVs reflected the antimicrobial and hemolytic activities of the copolymers. PB₃₆ formed pores on the lipid bilayer, and PM₃₄ and PM₅₇ caused GUVs to burst. These mechanisms are not dependent on the lipid types and appears to be inherent to the properties of hydrophobic groups. PM₃₄ and PM₅₇ showed characteristic sigmoid curves of the time course of GUV burst. We proposed a new kinetic model with a positive feedback in the formation of polymer aggregates, which is the rate determining step in GUV burst.

The novelty of our study lies in the finding of alkyl-dependent membrane-disrupting mechanisms of pore formation and membrane rupture, which is a stark contrast with AMPs. We expect that this finding will offer two following potential outcomes in our polymer design and medical applications: (1) a new insight into the role of hydrophobic groups in optimization strategy for antimicrobial activity and selectivity to maximize the therapeutic potential of antimicrobial polymers, and (2) an opportunity to regulate the membrane permeabilization at a molecular level toward precise control of cellular uptake of therapeutic molecules. While antimicrobial polymers have been investigated extensively in term of activity and chemical optimization, we believe that we have just begun to scratch the surface to understand the relationship between their structure, mechanism, and activity. To provide better links in the structure-activity relationship and for the rationale

design of the polymers, more studies will be needed using a comprehensive set of polymers with structural parameters and properties to understand the functional relationship between biological activity and membrane disruption.

ACKNOWLEDGMENTS

This work was supported in part by a Grant-in-aid for Young Scientists A (K. Y., No. 24681028) and Scientific Research (B) (K. Y., No. 18H03533) from the Japan Society for the Promotion of Science (JSPS), NSF (K. K., DMR-2004305, BMAT), and Support from Department of Biologic and Materials Sciences, University of Michigan School of Dentistry (K. K.).

Supporting information: Synthesis and characterization of the polymethacrylate derivatives, calculation of total cross-sectional area of pores, simulation of RITC-dextran leakage, schematic image of the chamber, time-course of FITC-dextran fluorescence, calibration curve for the relative gray value, and additional GUV images.

References

1. Takahashi, H.; Palermo, E.; Yasuhara, K.; Caputo, G.; Kuroda, K., Molecular Design, Structures, and Activity of Antimicrobial Peptide-Mimetic Polymers. *Macromol. Biosci.* **2013**, *13* (10), 1285-1299.

- 2. Takahashi, H.; Caputo, G.; Vemparala, S.; Kuroda, K., Synthetic Random Copolymers as a Molecular Platform To Mimic Host-Defense Antimicrobial Peptides. *Bioconj. Chem.* **2017**, *28* (5), 1340-1350.
- 3. Kenawy, E.; Worley, S.; Broughton, R., The chemistry and applications of antimicrobial polymers: A state-of-the-art review. *Biomacromolecules* **2007**, *8* (5), 1359-1384.
- 4. Engler, A.; Wiradharma, N.; Ong, Z.; Coady, D.; Hedrick, J.; Yang, Y., Emerging trends in macromolecular antimicrobials to fight multi-drug-resistant infections.

 Nano Today 2012, 7 (3), 201-222.
- 5. Tew, G.; Scott, R.; Klein, M.; Degrado, W., De Novo Design of Antimicrobial Polymers, Foldamers, and Small Molecules: From Discovery to Practical Applications. *Acc. Chem. Res.* **2010**, *43* (1), 30-39.
- Zasloff, M., Antimicrobial peptides of multicellular organisms. *Nature* 2002, 415 (6870), 389-395.
- 7. Brogden, K., Antimicrobial peptides: Pore formers or metabolic inhibitors in bacteria? *Nat. Rev. Microbiol.* **2005**, *3* (3), 238-250.
- 8. Makhlynets, O. V.; Caputo, G. A., Characteristics and therapeutic applications of antimicrobial peptides. *Biophys. Rev.* **2021**, *2* (1), 011301.
- 9. Sani, M. A.; Separovic, F., How Membrane-Active Peptides Get into Lipid Membranes. *Acc. Chem. Res.* **2016**, *49* (6), 1130-1138.
- 10. Kuroda, K.; DeGrado, W., Amphiphilic polymethacrylate derivatives as antimicrobial agents. *J. Am. Chem. Soc.* **2005**, *127* (12), 4128-4129.

- 11. Judzewitsch, P. R.; Corrigan, N.; Trujillo, F.; Xu, J.; Moad, G.; Hawker, C. J.; Wong, E. H. H.; Boyer, C., High-Throughput Process for the Discovery of Antimicrobial Polymers and Their Upscaled Production via Flow Polymerization. *Macromolecules* **2020**, *53* (2), 631-639.
- 12. Schaefer, S.; Pham, T. T. P.; Brunke, S.; Hube, B.; Jung, K.; Lenardon, M. D.; Boyer, C., Rational Design of an Antifungal Polyacrylamide Library with Reduced Host-Cell Toxicity. *ACS Appl. Mater. Interfaces* **2021**, *13* (23), 27430-27444.
- 13. King, A.; Chakrabarty, S.; Zhang, W.; Zeng, X. M.; Ohman, D. E.; Wood, L. F.; Abraham, S.; Rao, R.; Wynne, K. J., High Antimicrobial Effectiveness with Low Hemolytic and Cytotoxic Activity for PEG/Quaternary Copolyoxetanes.

 Biomacromolecules 2014, 15 (2), 456-467.
- 14. Mankoci, S.; Ewing, J.; Dalai, P.; Sahai, N.; Barton, H. A.; Joy, A., Bacterial Membrane Selective Antimicrobial Peptide-Mimetic Polyurethanes: Structure–Property Correlations and Mechanisms of Action. *Biomacromolecules* **2019**, *20* (11), 4096-4106.
- 15. Liu, L.; Courtney, K. C.; Huth, S. W.; Rank, L. A.; Weisblum, B.; Chapman, E. R.; Gellman, S. H., Beyond Amphiphilic Balance: Changing Subunit Stereochemistry Alters the Pore-Forming Activity of Nylon-3 Polymers. *J. Am. Chem. Soc.* **2021**, *143* (8), 3219-3230.
- 16. Mowery, B. P.; Lee, S. E.; Kissounko, D. A.; Epand, R. F.; Epand, R. M.; Weisblum, B.; Stahl, S. S.; Gellman, S. H., Mimicry of Antimicrobial Host-Defense Peptides by Random Copolymers. *J. Am. Chem. Soc.* **2007**, *129* (50), 15474-15476.

- 17. Colak, S.; Nelson, C. F.; Nüsslein, K.; Tew, G. N., Hydrophilic Modifications of an Amphiphilic Polynorbornene and the Effects on its Hemolytic and Antibacterial Activity. *Biomacromolecules* **2009**, *10* (2), 353-359.
- 18. Nimmagadda, A.; Liu, X.; Teng, P.; Su, M.; Li, Y.; Qiao, Q.; Khadka, N.; Sung, X.; Pan, J.; Xu, H.; Li, Q.; Cai, J., Polycarbonates with Potent and Selective Antimicrobial Activity toward Gram-Positive Bacteria. *Biomacromolecules* **2017**, *18* (1), 87-95.
- 19. Oda, Y.; Kanaoka, S.; Sato, T.; Aoshima, S.; Kuroda, K., Block versus Random Amphiphilic Copolymers as Antibacterial Agents. *Biomacromolecules* **2011**, *12* (10), 3581-3591.
- 20. Rauschenbach, M.; Lawrenson, S. B.; Taresco, V.; Pearce, A. K.; O'Reilly, R. K., Antimicrobial Hyperbranched Polymer–Usnic Acid Complexes through a Combined ROP-RAFT Strategy. *Macromol. Rapid Commun.* **2020**, *41* (18), 2000190.
- 21. Nederberg, F.; Zhang, Y.; Tan, J.; Xu, K.; Wang, H.; Yang, C.; Gao, S.; Guo, X.; Fukushima, K.; Li, L.; Hedrick, J.; Yang, Y., Biodegradable nanostructures with selective lysis of microbial membranes. *Nat. Chem.* **2011**, *3* (5), 409-414.
- 22. Nguyen, T.; Lam, S.; Ho, K.; Kumar, N.; Qiao, G.; Egan, S.; Boyer, C.; Wong, E., Rational Design of Single-Chain Polymeric Nanoparticles That Kill Planktonic and Biofilm Bacteria. *ACS Infect. Dis.* **2017**, *3* (3), 237-248.
- 23. Jhiang, J.; Wu, T.; Chou, C.; Chang, Y.; Huang, C., Gel-like ionic complexes for antimicrobial, hemostatic and adhesive properties. *J. Mat. Chem. B* **2019**, *7* (17), 2878-2887.

- 24. Kumar, A.; Boyer, C.; Nebhani, L.; Wong, E., Highly Bactericidal Macroporous Antimicrobial Polymeric Gel for Point-of-Use Water Disinfection. *Sci. Rep.* **2018**, *8*, 7965.
- 25. Ng, V. W. L.; Chan, J. M. W.; Sardon, H.; Ono, R. J.; Garcia, J. M.; Yang, Y. Y.; Hedrick, J. L., Antimicrobial hydrogels: A new weapon in the arsenal against multidrug-resistant infections. *Adv. Drug Deliv. Rev.* **2014**, *78*, 46-62.
- 26. Shai, Y., Mode of action of membrane active antimicrobial peptides. *Biopolymers* **2002**, *66* (4), 236-248.
- 27. Shai, Y.; Oren, Z., From "carpet" mechanism to de-novo designed diastereomeric cell-selective antimicrobial peptides. *Peptides* **2001**, *22* (10), 1629-1641.
- 28. Islam, M.; Alam, J.; Tamba, Y.; Karal, M.; Yamazaki, M., The single GUV method for revealing the functions of antimicrobial, pore-forming toxin, and cell-penetrating peptides or proteins. *Phys. Chem. Chem. Phys.* **2014**, *16* (30), 15752-15767.
- 29. Ambroggio, E.; Separovic, F.; Bowie, J.; Fidelio, G.; Bagatolli, L., Direct visualization of membrane leakage induced by the antibiotic peptides: Maculatin, citropin, and aurein. *Biophys. J.* **2005**, *89* (3), 1874-1881.
- 30. Domingues, T.; Riske, K.; Miranda, A., Revealing the Lytic Mechanism of the Antimicrobial Peptide Gomesin by Observing Giant Unilamellar Vesicles. *Langmuir* **2010**, *26* (13), 11077-11084.
- 31. Mally, M.; Majhenc, J.; Svetina, S.; Zeks, B., The response of giant phospholipid vesicles to pore-forming peptide melittin. *Biochim. Biophys. Acta Biomembr.* **2007**, *1768* (5), 1179-1189.

- 32. Lee, M.; Sun, T.; Hung, W.; Huang, H., Process of inducing pores in membranes by melittin. *Proc. Natl. Acad. Sci. U. S. A.* **2013**, *110* (35), 14243-14248.
- 33. Lee, M. T.; Hung, W. C.; Chen, F. Y.; Huang, H. W., Mechanism and kinetics of pore formation in membranes by water-soluble amphipathic peptides. *Proc. Natl. Acad. Sci. U. S. A.* **2008**, *105* (13), 5087-5092.
- 34. Hasan, M.; Karal, M.; Levadnyy, V.; Yamazaki, M., Mechanism of Initial Stage of Pore Formation Induced by Antimicrobial Peptide Magainin 2. *Langmuir* **2018**, *34* (10), 3349-3362.
- 35. Karal, M.; Alam, J.; Takahashi, T.; Levadny, V.; Yamazaki, M., Stretch-Activated Pore of the Antimicrobial Peptide, Magainin 2. *Langmuir* **2015**, *31* (11), 3391-3401.
- 36. Tamba, Y.; Yamazaki, M., Single giant unilamellar vesicle method reveals effect of antimicrobial peptide magainin 2 on membrane permeability. *Biochemistry* **2005**, *44* (48), 15823-15833.
- 37. Tamba, Y.; Yamazaki, M., Magainin 2-Induced Pore Formation in the Lipid Membranes Depends on Its Concentration in the Membrane Interface. *J.Phys. Chem. B* **2009**, *113* (14), 4846-4852.
- 38. Lee, C.; Sun, Y.; Chen, C.; Qian, S.; Huang, H., Transmembrane Pores Formed by Human Antimicrobial Peptide LL-37. *Biophys. J.* **2011**, *100* (3), 336-336.
- 39. Vial, F.; Cousin, F.; Bouteiller, L.; Tribet, C., Rate of Permeabilization of Giant Vesicles by Amphiphilic Polyacrylates Compared to the Adsorption of These Polymers onto Large Vesicles and Tethered Lipid Bilayers. *Langmuir* **2009**, *25* (13), 7506-7513.
 - 40. National Committee for Clinical Laboratory Standards. Methods for

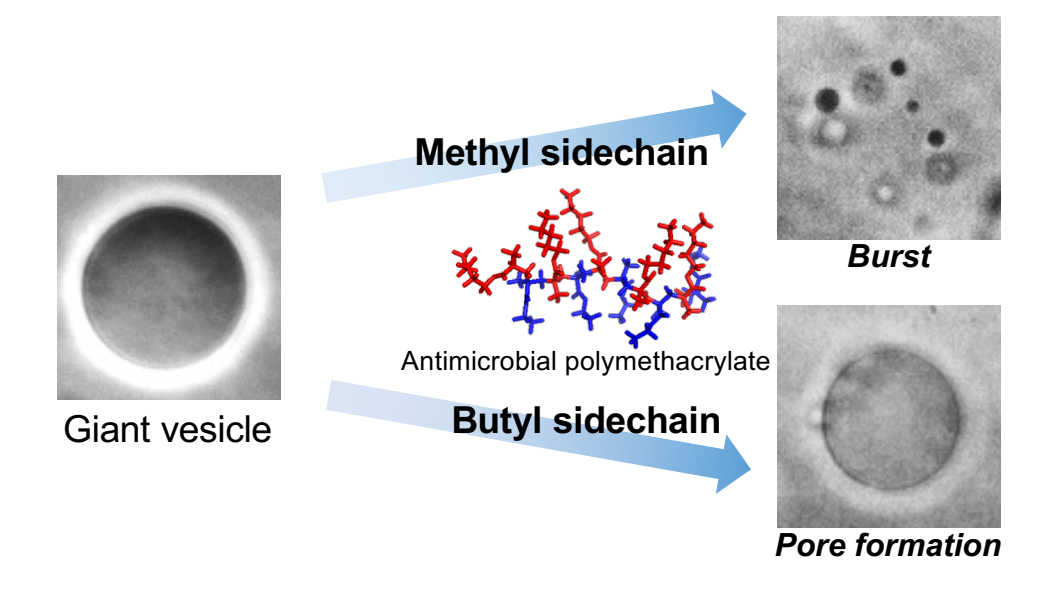
- dilution antimicrobial susceptibility tests for bacteria that grow aerobically. NCCLS, Ed. Villanova, PA, 2003.
- 41. Reeves, J. P.; Dowben, R. M., Formation and properties of thin-walled phospholipid vesicles. *J. Cell Physiol.* **1969**, *73* (1), 49-60.
- 42. Foster, L. L.; Mizutani, M.; Oda, Y.; Palermo, E. F.; Kuroda, K., Design and Synthesis of Amphiphilic Vinyl Copolymers with Antimicrobial Activity. In *Polymers for Biomedicine*, 2017; pp 243-272.
- 43. Kuroda, K.; Caputo, G.; DeGrado, W., The Role of Hydrophobicity in the Antimicrobial and Hemolytic Activities of Polymethacrylate Derivatives. *Chem. Eur. J.* **2009**, *15* (5), 1123-1133.
- 44. Raetz, C. R.; Dowhan, W., Biosynthesis and function of phospholipids in Escherichia coli. *J. Biol. Chem.* **1990**, *265* (3), 1235-1238.
- 45. Akashi, K.; Miyata, H.; Itoh, H.; Kinosita, K., Preparation of giant liposomes in physiological conditions and their characterization under an optical microscope. *Biophys. J.* **1996**, *71* (6), 3242-3250.
- 46. Horger, K. S.; Estes, D. J.; Capone, R.; Mayer, M., Films of agarose enable rapid formation of giant liposomes in solutions of physiologic ionic strength. *J. Am. Chem. Soc.* **2009**, *131* (5), 1810-1819.
- 47. Shum, H. C.; Lee, D.; Yoon, I.; Kodger, T.; Weitz, D. A., Double emulsion templated monodisperse phospholipid vesicles. *Langmuir* **2008**, *24* (15), 7651-7653.
- 48. Brochard-Wyart, F.; de Gennes, P.; Sandre, O., Transient pores in stretched vesicles: role of leak-out. *Physica a* **2000**, *278* (1-2), 32-51.

- 49. Sandre, O.; Moreaux, L.; Brochard-Wyart, F., Dynamics of transient pores in stretched vesicles. *Proc. Natl. Acad. Sci. U. S. A.* **1999,** *96* (19), 10591-10596.
- 50. Mathlouthi, M.; Reiser, P., *Sucrose : properties and applications*. Blackie Academic & Professional: London, 1995.
- 51. Baul, U.; Kuroda, K.; Vemparala, S., Interaction of multiple biomimetic antimicrobial polymers with model bacterial membranes. *J. Chem. Phys.* **2014**, *141* (8), 084902.
- 52. Palermo, E. F.; Vemparala, S.; Kuroda, K., Cationic spacer arm design strategy for control of antimicrobial activity and conformation of amphiphilic methacrylate random copolymers. *Biomacromolecules* **2012**, *13* (5), 1632-1641.
- 53. Sani, M. A.; Gagne, E.; Gehman, J. D.; Whitwell, T. C.; Separovic, F., Dye-release assay for investigation of antimicrobial peptide activity in a competitive lipid environment. *Eur. Biophys. J.* **2014**, *43* (8-9), 445-450.
- 54. Chen, F. Y.; Lee, M. T.; Huang, H. W., Sigmoidal concentration dependence of antimicrobial peptide activities: a case study on alamethicin. *Biophys. J.* **2002**, *82* (2), 908-914.
- 55. Rautenbach, M.; Gerstner, G. D.; Vlok, N. M.; Kulenkampff, J.; Westerhoff, H. V., Analyses of dose-response curves to compare the antimicrobial activity of model cationic alpha-helical peptides highlights the necessity for a minimum of two activity parameters. *Anal. Biochem.* **2006**, *350* (1), 81-90.
- 56. Bissette, A.; Fletcher, S., Mechanisms of Autocatalysis. *Angew. Chem. Int. Ed.* **2013**, *52* (49), 12800-12826.

- 57. Plasson, R.; Brandenburg, A.; Jullien, L.; Bersini, H., Autocatalyses. *J. Phys. Chem. A* **2011**, *115* (28), 8073-8085.
- 58. Schuster, P., What is special about autocatalysis? *Monatshefte Fur Chemie* **2019**, *150* (5), 763-775.
- 59. Burnham, A., Use and misuse of logistic equations for modeling chemical kinetics. *J. Therm. Anal. Calorim.* **2017**, *127* (1), 1107-1116.
- 60. Teixeira, V.; Feio, M. J.; Bastos, M., Role of lipids in the interaction of antimicrobial peptides with membranes. *Progress in Lipid Research* **2012**, *51* (2), 149-177.
- 61. Tamba, Y.; Ariyama, H.; Levadny, V.; Yamazaki, M., Kinetic Pathway of Antimicrobial Peptide Magainin 2-Induced Pore Formation in Lipid Membranes. *J.Phys. Chem. B* **2010**, *114* (37), 12018-12026.
- 62. Sudbrack, T. P.; Archilha, N. L.; Itri, R.; Riske, K. A., Observing the solubilization of lipid bilayers by detergents with optical microscopy of GUVs. *J. Phys. Chem. B* **2011**, *115* (2), 269-277.
- 63. Yasuhara, K.; Arakida, J.; Ravula, T.; Ramadugu, S.; Sahoo, B.; Kikuchi, J.; Ramamoorthy, A., Spontaneous Lipid Nanodisc Fomation by Amphiphilic Polymethacrylate Copolymers. *Journal of the American Chemical Society* **2017**, *139* (51), 18657-18663.
- 64. Toraya, S.; Nagao, T.; Norisada, K.; Tuzi, S.; Saito, H.; Izumi, S.; Naito, A., Morphological behavior of lipid bilayers induced by melittin near the phase transition temperature. *Biophys. J.* **2005**, *89* (5), 3214-3222.

- 65. Matsuzaki, K.; Sugishita, K.; Fujii, N.; Miyajima, K., Molecular basis for membrane selectivity of an antimicrobial peptide, magainin 2. *Biochemistry* **1995**, *34* (10), 3423-3429.
- 66. Hernández-Villa, L.; Manrique-Moreno, M.; Leidy, C.; Jemioła-Rzemińska, M.; Ortíz, C.; Strzałka, K., Biophysical evaluation of cardiolipin content as a regulator of the membrane lytic effect of antimicrobial peptides. *Biophys. Chem.* **2018**, *238*, 8-15.
- 67. Kubiak, J.; Brewer, J.; Hansen, S.; Bagatolli, L. A., Lipid lateral organization on giant unilamellar vesicles containing lipopolysaccharides. *Biophys. J.* **2011**, *100* (4), 978-986.
- 68. Montes, L.; Alonso, A.; Goni, F.; Bagatolli, L., Giant unilamellar vesicles electroformed from native membranes and organic lipid mixtures under physiological conditions. *Biophys. J.* **2007**, *93* (10), 3548-3554.
- 69. Baumgart, T.; Hammond, A. T.; Sengupta, P.; Hess, S. T.; Holowka, D. A.; Baird, B. A.; Webb, W. W., Large-scale fluid/fluid phase separation of proteins and lipids in giant plasma membrane vesicles. *Proc. Natl. Acad. Sci. U. S. A.* **2007**, *104* (9), 3165-3170.
- 70. Avery, C.; Palermo, E.; McLaughin, A.; Kuroda, K.; Chen, Z., Investigations of the Interactions between Synthetic Antimicrobial Polymers and Substrate-Supported Lipid Bilayers Using Sum Frequency Generation Vibrational Spectroscopy. *Anal. Chem.* **2011**, *83* (4), 1342-1349.
- 71. Epand, R. M.; Rotem, S.; Mor, A.; Berno, B.; Epand, R. F., Bacterial membranes as predictors of antimicrobial potency. *J. Am. Chem. Soc.* **2008**, *130* (43), 14346-14352.

- 72. Hu, K.; Schmidt, N.; Zhu, R.; Jiang, Y.; Lai, G.; Wei, G.; Palermo, E.; Kuroda, K.; Wong, G.; Yang, L., A Critical Evaluation of Random Copolymer Mimesis of Homogeneous Antimicrobial Peptides. *Macromolecules* **2013**, *46* (5), 1908-1915.
- 73. Leite, N.; Aufderhorst-Roberts, A.; Palma, M.; Connell, S.; Neto, J.; Beales, P., PE and PS Lipids Synergistically Enhance Membrane Poration by a Peptide with Anticancer Properties. *Biophys. J.* **2015**, *109* (5), 936-947.
- 74. Paterson, D.; Tassieri, M.; Reboud, J.; Wilson, R.; Cooper, J., Lipid topology and electrostatic interactions underpin lytic activity of linear cationic antimicrobial peptides in membranes. *Proc. Natl. Acad. Sci. U. S. A.* **2017**, *114* (40), E8324-E8332.
- 75. Palermo, E. F.; Sovadinova, I.; Kuroda, K., Structural determinants of antimicrobial activity and biocompatibility in membrane-disrupting methacrylamide random copolymers. *Biomacromolecules* **2009**, *10* (11), 3098-3107.
- 76. Mant, C. T.; Jiang, Z.; Gera, L.; Davis, T.; Nelson, K. L.; Bevers, S.; Hodges, R. S., De Novo Designed Amphipathic α-Helical Antimicrobial Peptides Incorporating Dab and Dap Residues on the Polar Face To Treat the Gram-Negative Pathogen, Acinetobacter baumannii. *J. Med. Chem.* **2019**, *62* (7), 3354-3366.
- 77. Hitchner, M. A.; Santiago-Ortiz, L. E.; Necelis, M. R.; Shirley, D. J.; Palmer, T. J.; Tarnawsky, K. E.; Vaden, T. D.; Caputo, G. A., Activity and characterization of a pH-sensitive antimicrobial peptide. *Biochim. Biophys. Acta Biomembr.* **2019**, *1861* (10), 182984.
- 78. Arias, M.; Piga, K. B.; Hyndman, M. E.; Vogel, H. J., Improving the Activity of Trp-Rich Antimicrobial Peptides by Arg/Lys Substitutions and Changing the Length of Cationic Residues. *Biomolecules* **2018**, *8* (2), 19.



TOC Graphic